Strange hadronic matter in a fully self-consistent mean-field model*

K. Miyazaki

Abstract

A new relativistic mean-field model of baryon matter is developed. It is constructed by modifying the Zimanyi-Moszkowski model based on the constituent quark picture of baryons and is further extended so as to take into account the (hidden) strange mesons. The model is applied to dense strange hadronic matter using three sets of hyperon-hyperon interactions. The first one is characterized by strong $\Lambda\Lambda$ attraction, the second has weak $\Lambda\Lambda$ but strong $\Sigma\Sigma$ attraction and in the third set both the interactions are weak. There have been found in all the sets the most stable forms of baryon matter with the deeper binding-energies than the saturation energy of normal nuclear matter and the strangeness fractions being larger than 1. Their properties are dominated by the abundance of Λ, Σ and Ξ hyperons respectively for each set of interactions. In the comparisons with the nonlinear Walecka and the modified quark-meson coupling model, we have confirmed that it is important to take precisely into account the medium dependences of effective meson-baryon coupling constants in dense baryon matter.

1 Introduction

One of the greatest interests in recent nuclear physics is the dense hadronic matter with large strangeness fraction. Such an object may be realized in the high-energy heavy-ion collisions on the terrestrial laboratory or in the core region of neutron stars. In theoretical aspect it has therefore become an important subject to develop the reasonable models of dense hadronic matter. We generally expect that the baryons in dense medium overlap with each other and lose partially their identities and then the phase transition to quark matter occurs above some critical density. Ones expect that the density has relatively low value, a few times of the nuclear saturation density, but we have no reliable information on it. Inversely speaking the reasonable description of dense hadronic matter in a picture of baryons and mesons is crucial to decide the precise value of the critical density.

Although there are a great variety of the models for dense baryonic matter, the relativistic mean-field (RMF) theories based on or inspired by the Walecka model [1] are most promising. Nevertheless we still have several variants even in this sphere. The most

*This paper is the revised version of CDS ext-2004-071 in which there has been found a bug in numerical code. Although the revisions of the results in figures are not substantial, the analyses in section 3 have been refined to some extent. I have also corrected several unclear contexts and mistypes.

widely used model is an extension of the Walecka model to include the nonlinear meson self-coupling terms [2], hereafter called the NLW model. It is however noted that many parameters in the model are adjusted to reproduce the properties of normal nuclear matter and finite nuclei. Consequently, the NLW model is really valid around the nuclear saturation density, but there are no guarantees that it is meaningful at high densities.

In this respect the models embodying the density-dependence are desired. One of such efforts is the density-dependent hadron field (DDRH) theory [3]. It is however based on the Dirac-Brueckner-Hartree-Fock (DBHF) theory [4] and we have no realistic DBHF calculations of baryonic matter including hyperons at present in contrast to the non-relativistic Brueckner-Hartree-Fock (NRBHF) calculations [5,6]. As a result the density dependence of meson-hyperon vertices in the DDRH model cannot be well determined.

We therefore arrive at a conclusion that the RMF models, which have implicit density dependence through the effective masses of baryons in the medium but are independent of the DBHF theory, are more desired. One of such models is the quark-meson coupling (QMC) model [7]. It is based on the bag model of baryons and the first attempt to unify the RMF model of baryonic matter and baryon structure. The density dependence in the QMC model indeed results from baryon structure in the medium.

Within an extension of the Walecka model, Zimanyi and Moszkowski (ZM) [8] developed another model embodying implicit density-dependence. It employs the effective renormalized $NN\sigma$ coupling constant $g^*_{NN\sigma} = (M^*_N/M_N)\, g_{NN\sigma}$ where M^*_N is the effective mass of a nucleon in nuclear medium. The ZM model however has the defect that it cannot reproduce the strong spin-orbit potentials because of its larger effective mass $M^*_N \simeq 0.86 M_N$ than the reasonable empirical value $M^*_N \simeq 0.6 M_N$. In addition, its extension to hyperons cannot be determined in unique way [9,10].

Here it is noted that the ZM model predicted the similar saturation properties of nuclear matter to the QMC model. Both the models have effectively density-dependent $NN\sigma$ coupling constant. This suggests that the ZM model has its theoretical foundation on the nucleon structure. In fact it has been shown [11] that the relativistic SU(6) model of a nucleon gives the similar $NN\sigma$ coupling to the ZM model. Reference [12] investigated the renormalization of wave function in the Walecka model so as to take into account the nucleon structure in terms of the meson cloud in nuclear medium. We have obtained the improved ZM model, which includes effectively density-dependent $NN\omega$ coupling as well as $NN\sigma$ coupling. The predicted nuclear matter saturation properties are comparable to the DBHF calculation.

Furthermore it has been recently found [13] that 1) the ZM model can be interpreted from the constituent quark picture of nucleons, 2) the renormalized $NN\sigma$ coupling results from the effect of scalar potential on the quarks and 3) a slight modification of the ZM model reproduces almost the same result as Ref. [12]. Because this modified ZM (MZM) model can be extended to meson-hyperons couplings unambiguously, it has readily applied to the strange hadronic matter (SHM).

Although the MZM model has been further applied to the asymmetric nuclear matter [14], the neutron star matter [15] and the s-wave antikaon condensations in neutron stars [16], they take into account only the interactions between nonstrange quarks. This is because we have little information on the interactions between hyperons. However the precise description of YY interactions really requires the interactions between s quarks. The purpose of the present work is to extend the investigation of Ref. [13] by including the (hidden) strange mesons according to Refs. [17,18].

In the next section we first develop the effective renormalized meson-baryon coupling constants in the mean-fields by scalar σ and strange scalar σ^* mesons and then the RMF description of SHM. In section 3 the properties of SHM are calculated and our results are compared with the most refined NLW model [18] and the modified QMC model [19]. Finally we summarize our investigations and draw conclusions in section 4.

2 Formalism

In this work we investigate charge-symmetric baryon matter and so take into account only the isoscalar σ and ω mesons and their strange counterparts σ^* and ϕ mesons. Their masses are $m_\sigma = 550\,\mathrm{MeV}$, $m_\omega = 783\,\mathrm{MeV}$, $m_{\sigma^*} = 975\,\mathrm{MeV}$ and $m_\phi = 1020\,\mathrm{MeV}$. The masses of baryons are assumed to be $M_N = 938.9\,\mathrm{MeV}$, $M_\Lambda = 1115.6\,\mathrm{MeV}$, $M_\Sigma = 1193.05\,\mathrm{MeV}$ and $M_\Xi = 1318.1\,\mathrm{MeV}$.

2.1 Effective renormalized coupling constants

In order to clarify the basic concept of our model, we first review the effective meson-nucleon coupling constants derived in Ref. [13]. In the constituent quark model (QCM) of a nucleon, the free $NN\sigma$ or $NN\omega$ coupling used in the Walecka model is depicted by

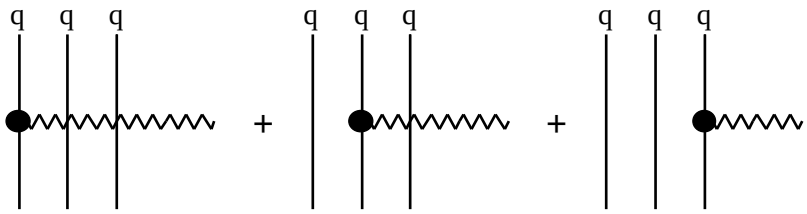

or the coupling constant is expressed by

$$g_{NN\sigma(\omega)} = 3\, g^{(N)}_{qq\sigma(\omega)}. \tag{1}$$

Here only one quark $q = u$ or d in a nucleon couples to the mesons (the wavy lines) but the other two quarks are spectators. However for a nucleon in medium all the three quarks are embedded in meson mean-fields. This effect should be taken into account so

as to go beyond the Walecka model. The QMC model [7] was inspired by the same idea, in which the mean-fields fulfill a nucleon bag.

Then we have considered the following first-order medium correction:

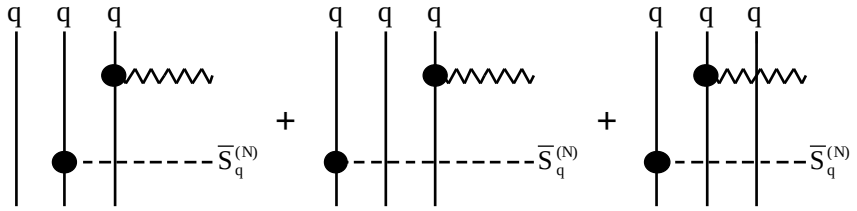

where $\bar{S}_q^{(N)} \equiv S_q^{(N)}/M_N = S_N/(3M_N)$ is the effect by scalar potential on a quark in nucleon. Hereafter we use the symbols S_B, $S_q^{(B)}$ and $S_s^{(B)}$ for the scalar potentials of baryon B, its constituent u or d quark and its s quark. Adding these contributions to Eq. (1), we have the effective $NN\sigma(\omega)$ coupling constant

$$g^*_{NN\sigma(\omega)} = g_{NN\sigma(\omega)} + 3\,\bar{S}_q^{(N)} g^{(N)}_{qq\sigma(\omega)} = \left(1 + \frac{1}{3}\frac{S_N}{M_N}\right) g_{NN\sigma(\omega)} = \left[(1-\lambda_N) + \lambda_N m^*_N\right] g_{NN\sigma(\omega)}, \tag{2}$$

where $m^*_N = M^*_N/M_N = (M_N + S_N)/M_N$ and $\lambda_N = 1/3$. If $\bar{S}_q^{(N)}$ in the above figure is replaced by $S_q^{(N)}/M_q$, where $M_q = (1/3)\,M_N$ is the mass of a constituent quark, the original ZM model ($\lambda_N = 1$) is recovered. In Ref. [13] we first interpreted the ZM model from the QCM of nucleons and then modified it as in Eq. (2).

It is straightforward to extend the above consideration of meson-nucleon coupling to meson-hyperons couplings including the contributions of strange mesons. The free $\Lambda\Lambda\sigma$ or $\Lambda\Lambda\omega$ coupling in the QCM is depicted by

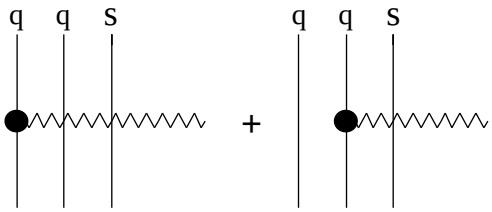

or the coupling constant is expressed by

$$g_{\Lambda\Lambda\sigma(\omega)} = 2\,g^{(\Lambda)}_{qq\sigma(\omega)}. \tag{3}$$

This is corrected by the medium contributions,

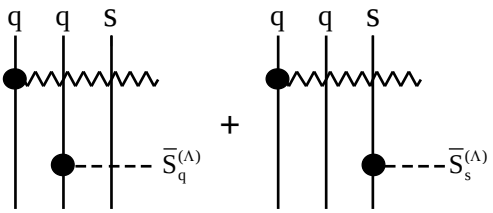

where $\bar{S}_q^{(\Lambda)} \equiv S_q^{(\Lambda)}/M_\Lambda$ and $\bar{S}_s^{(\Lambda)} \equiv S_s^{(\Lambda)}/M_\Lambda$ are the effects of scalar potentials on the constituent u or d and s quark in Λ. Consequently, we have the effective $\Lambda\Lambda\sigma(\omega)$ coupling constant

$$g^*_{\Lambda\Lambda\sigma(\omega)} = g_{\Lambda\Lambda\sigma(\omega)} + \left(\bar{S}_q^{(\Lambda)} + \bar{S}_s^{(\Lambda)}\right) g^{(\Lambda)}_{qq\sigma(\omega)} = \left[1 + \frac{1}{2}\left(\bar{S}_q^{(\Lambda)} + \bar{S}_s^{(\Lambda)}\right)\right] g_{\Lambda\Lambda\sigma(\omega)}. \tag{4}$$

If $\bar{S}_s^{(\Lambda)}$ is neglected, Eq. (6) in Ref. [13] is recovered.

The effective $\Lambda\Lambda\sigma^*$ or $\Lambda\Lambda\phi$ coupling in the mean-fields is obviously given by

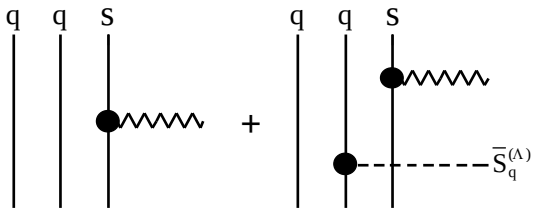

or the renormalized coupling constant is expressed by

$$g^*_{\Lambda\Lambda\sigma^*(\phi)} = \left(1 + \bar{S}_q^{(\Lambda)}\right) g_{\Lambda\Lambda\sigma^*(\phi)}. \tag{5}$$

Because there are no isovector mean-fields in the present work, the renormalized meson-Σ coupling constants have the same forms as Λ:

$$g^*_{\Sigma\Sigma\sigma(\omega)} = \left[1 + \frac{1}{2}\left(\bar{S}_q^{(\Sigma)} + \bar{S}_s^{(\Sigma)}\right)\right] g_{\Sigma\Sigma\sigma(\omega)}, \tag{6}$$

$$g^*_{\Sigma\Sigma\sigma^*(\phi)} = \left(1 + \bar{S}_q^{(\Sigma)}\right) g_{\Sigma\Sigma\sigma^*(\phi)}. \tag{7}$$

The most prominent difference between the MZM model in Ref. [13] without the strange mesons and the present extended version including them is apparent in the meson-Ξ couplings. Only taking into account the strange mesons is able to renormalize the coupling constants because Ξ's contain only one u or d quark. In fact the effective $\Xi\Xi\sigma$ or $\Xi\Xi\omega$ coupling in the mean-fields is given by

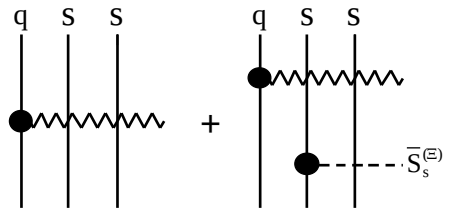

or the renormalized coupling constant is expressed by

$$g^*_{\Xi\Xi\sigma(\omega)} = \left(1 + \bar{S}_s^{(\Xi)}\right) g_{\Xi\Xi\sigma(\omega)}, \tag{8}$$

where $\bar{S}_s^{(\Xi)} \equiv S_s^{(\Xi)}/M_\Xi$ is the effect of scalar potential on the s-quark in Ξ's.

Next, the free $\Xi\Xi\sigma^*$ or $\Xi\Xi\phi$ coupling in the QCM is depicted by

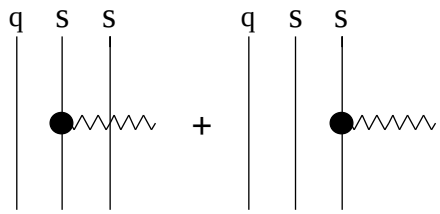

or the coupling constant is given by

$$g_{\Xi\Xi\sigma^*(\phi)} = 2\, g^{(\Xi)}_{ss\sigma^*(\phi)}. \tag{9}$$

The medium correction to this is depicted by

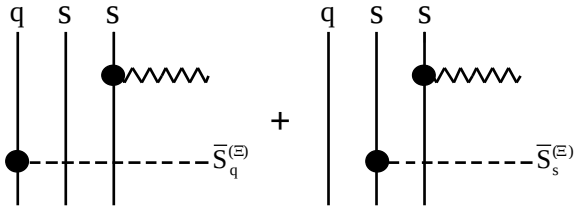

where $\bar{S}_q^{(\Xi)} \equiv S_q^{(\Xi)}/M_\Xi$ is the effect of scalar potential on the constituent u or d quark in Ξ^0 or Ξ^-. Consequently, we have the renormalized $\Xi\Xi\sigma^*(\phi)$ coupling constant

$$g^*_{\Xi\Xi\sigma^*(\phi)} = g_{\Xi\Xi\sigma^*(\phi)} + \left(\bar{S}_q^{(\Xi)} + \bar{S}_s^{(\Xi)}\right) g^{(\Xi)}_{ss\sigma^*(\phi)} = \left[1 + \frac{1}{2}\left(\bar{S}_q^{(\Xi)} + \bar{S}_s^{(\Xi)}\right)\right] g_{\Xi\Xi\sigma^*(\phi)}. \tag{10}$$

Although we have derived the effective renormalized meson-baryon coupling constants in the intuitive schematic methods, their stringent derivations based on the relativistic SU(6) model of baryons will be presented in a future work including the contributions by isovector mesons.

2.2 The relativistic mean-field model of SHM

The relativistic mean-field Lagrangian of baryon matter is generally given by

$$\begin{aligned}\mathcal{L} &= \sum_{B=N,\Lambda,\Sigma,\Xi} \bar{\psi}_B \left(\not{p}_B - M_B^* - \gamma^0 V_B\right) \psi_B - \frac{1}{2} m_\sigma^2 \langle\sigma\rangle^2 - \frac{1}{2} m_{\sigma^*}^2 \langle\sigma^*\rangle^2 \\ &\quad + \frac{1}{2} m_\omega^2 \langle\omega_0\rangle^2 + \frac{1}{2} m_\phi^2 \langle\phi_0\rangle^2,\end{aligned} \tag{11}$$

where $M_B^* = M_B + S_B$ and V_B are the effective mass and vector potential of each baryon:

$$S_B = -\, g^*_{BB\sigma} \langle\sigma\rangle - g^*_{BB\sigma^*} \langle\sigma^*\rangle\,, \tag{12}$$

$$V_B = g^*_{BB\omega} \langle\omega_0\rangle + g^*_{BB\phi} \langle\phi_0\rangle\,. \tag{13}$$

The energy density is given by

$$\mathcal{E} = \sum_{B=N,\Lambda,\Sigma,\Xi} \left(\langle E_k^* \rangle_B + V_B \right) \rho_B + \frac{1}{2} m_\sigma^2 \langle \sigma \rangle^2 + \frac{1}{2} m_{\sigma^*}^2 \langle \sigma^* \rangle^2 - \frac{1}{2} m_\omega^2 \langle \omega_0 \rangle^2 - \frac{1}{2} m_\phi^2 \langle \phi_0 \rangle^2 , \tag{14}$$

where $\langle E_k^* \rangle_B$ is the average kinetic energy and ρ_B is the density of each baryon. Inverting Eq. (13) we can express the vector mean-fields $\langle \omega_0 \rangle$ and $\langle \phi_0 \rangle$ by the vector potentials V_N and V_Λ, and so V_Σ and V_Ξ are also expressed by them. Therefore the energy density contains only V_N and V_Λ. Then, extremizing the energy $\partial \mathcal{E} / \partial V_N = \partial \mathcal{E} / \partial V_\Lambda = 0$, we have the general expression of vector potential

$$V_B = \frac{g_{BB\omega}^*}{m_\omega} \sum_{B'} \frac{g_{B'B'\omega}^*}{m_\omega} \rho_{B'} + \frac{g_{BB\phi}^*}{m_\phi} \sum_Y \frac{g_{YY\phi}^*}{m_\phi} \rho_Y, \tag{15}$$

and vector mean-fields

$$m_\omega^2 \langle \omega_0 \rangle = \sum_{B=N,\Lambda,\Sigma,\Xi} g_{BB\omega}^* \rho_B, \tag{16}$$

$$m_\phi^2 \langle \phi_0 \rangle = \sum_{Y=\Lambda,\Sigma,\Xi} g_{YY\phi}^* \rho_Y. \tag{17}$$

Substituting Eqs. (15)-(17) into (14), the energy density becomes

$$\mathcal{E} = \sum_B \langle E_k^* \rangle_B \rho_B + \frac{1}{2} m_\sigma^2 \langle \sigma \rangle^2 + \frac{1}{2} m_{\sigma^*}^2 \langle \sigma^* \rangle^2 + \frac{1}{2} \left(\sum_B \frac{g_{BB\omega}^*}{m_\omega} \rho_B \right)^2 + \frac{1}{2} \left(\sum_Y \frac{g_{YY\phi}^*}{m_\phi} \rho_Y \right)^2 . \tag{18}$$

This equation is a function of the effective masses of N and Λ as shown below.

First, because the scalar potential of nucleon is

$$S_N = - g_{NN\sigma}^* \langle \sigma \rangle = - \left[(1 - \lambda_N) + \lambda_N m_N^* \right] g_{NN\sigma} \langle \sigma \rangle , \tag{19}$$

the σ mean-field is expressed by the effective mass of nucleon as

$$\langle \sigma \rangle = \frac{M_N}{g_{NN\sigma}} \frac{1 - m_N^*}{(1 - \lambda_N) + \lambda_N m_N^*}. \tag{20}$$

Next, the scalar potential of Λ is given by

$$S_\Lambda = 2 S_q^{(\Lambda)} + S_s^{(\Lambda)}, \tag{21}$$

where

$$2 S_q^{(\Lambda)} = - g_{\Lambda\Lambda\sigma}^* \langle \sigma \rangle = - \left[1 + \frac{1}{2} \left(\bar{S}_q^{(\Lambda)} + \bar{S}_s^{(\Lambda)} \right) \right] g_{\Lambda\Lambda\sigma} \langle \sigma \rangle , \tag{22}$$

$$S_s^{(\Lambda)} = -\, g^*_{\Lambda\Lambda\sigma^*} \langle \sigma^* \rangle = -\left(1 + \bar{S}_q^{(\Lambda)}\right) g_{\Lambda\Lambda\sigma^*} \langle \sigma^* \rangle \,. \tag{23}$$

From Eqs. (22) and (23) the scalar potentials for the constituent quarks of Λ are expressed by

$$\bar{S}_q^{(\Lambda)} = -\,\frac{1 - \frac{1}{2}\,\bar{\sigma}^*_\Lambda}{C_\Lambda}\,\bar{\sigma}_\Lambda, \tag{24}$$

$$\bar{S}_s^{(\Lambda)} = -\,\frac{2 - \frac{1}{2}\,\bar{\sigma}_\Lambda}{C_\Lambda}\,\bar{\sigma}^*_\Lambda, \tag{25}$$

where we have introduced the reduced scalar mean-fields for each baryon,

$$\bar{\sigma}_B \equiv \frac{g_{BB\sigma}}{M_B} \langle \sigma \rangle \,, \qquad \bar{\sigma}^*_Y \equiv \frac{g_{YY\sigma^*}}{M_Y} \langle \sigma^* \rangle \,, \tag{26}$$

and

$$C_\Lambda = 2 + \frac{1}{2}\,(1 - \bar{\sigma}^*_\Lambda)\,\bar{\sigma}_\Lambda. \tag{27}$$

Therefore the renormalized $\Lambda\Lambda\sigma(\omega)$ and $\Lambda\Lambda\sigma^*(\phi)$ coupling constants are determined by

$$1 + \frac{1}{2}\left(\bar{S}_q^{(\Lambda)} + \bar{S}_s^{(\Lambda)}\right) = \frac{2 - \bar{\sigma}^*_\Lambda}{C_\Lambda}, \tag{28}$$

$$1 + \bar{S}_q^{(\Lambda)} = \frac{2 - \frac{1}{2}\,\bar{\sigma}_\Lambda}{C_\Lambda}. \tag{29}$$

Substituting Eqs. (24) and (25) into Eq. (21), we have

$$1 - m^*_\Lambda = \frac{2\left(1 - \frac{1}{2}\,\bar{\sigma}^*_\Lambda\right)\bar{\sigma}_\Lambda + \left(2 - \frac{1}{2}\,\bar{\sigma}_\Lambda\right)\bar{\sigma}^*_\Lambda}{C_\Lambda}. \tag{30}$$

Consequently,

$$\bar{\sigma}^*_\Lambda = \frac{2\,(1 - m^*_\Lambda) - \left[\,2 - \frac{1}{2}\,(1 - m^*_\Lambda)\right]\bar{\sigma}_\Lambda}{2 - \frac{1}{2}\,(2 + m^*_\Lambda)\,\bar{\sigma}_\Lambda}. \tag{31}$$

As seen from Eqs. (20) and (26), the $\bar{\sigma}_\Lambda$ is a function of m^*_N and so the $\bar{\sigma}^*_\Lambda$ depends on both of m^*_N and m^*_Λ.

On the analogies of Eqs. (28) and (29), the renormalized $\Sigma\Sigma\sigma(\omega)$ and $\Sigma\Sigma\sigma^*(\phi)$ coupling constants are determined by

$$1 + \frac{1}{2}\left(\bar{S}_q^{(\Sigma)} + \bar{S}_s^{(\Sigma)}\right) = \frac{2 - \bar{\sigma}^*_\Sigma}{C_\Sigma}, \tag{32}$$

$$1 + \bar{S}_q^{(\Sigma)} = \frac{2 - \frac{1}{2}\,\bar{\sigma}_\Sigma}{C_\Sigma}, \tag{33}$$

where

$$C_\Sigma = 2 + \frac{1}{2}\,(1 - \bar{\sigma}^*_\Sigma)\,\bar{\sigma}_\Sigma. \tag{34}$$

In addition, on the analogy of Eq. (30), the effective mass of Σ becomes

$$m^*_\Sigma = \frac{2 - \frac{3}{2}\,\bar{\sigma}_\Sigma - 2\,\bar{\sigma}^*_\Sigma + \bar{\sigma}_\Sigma\,\bar{\sigma}^*_\Sigma}{C_\Sigma}. \tag{35}$$

Because $\bar{\sigma}^*_\Sigma$ is expressed by $\bar{\sigma}^*_\Lambda$, Eqs. (32)-(35) are the functions of m^*_N and m^*_Λ.

Similarly the renormalized $\Xi\Xi\sigma(\omega)$ and $\Xi\Xi\sigma^*(\phi)$ coupling constants are determined by

$$1 + \bar{S}^{(\Xi)}_s = \frac{2 - \frac{1}{2}\,\bar{\sigma}^*_\Xi}{C_\Xi}, \tag{36}$$

$$1 + \frac{1}{2}\left(\bar{S}^{(\Xi)}_q + \bar{S}^{(\Xi)}_s\right) = \frac{2 - \bar{\sigma}_\Xi}{C_\Xi}, \tag{37}$$

and the effective mass of Ξ becomes

$$m^*_\Xi = \frac{2 - 2\,\bar{\sigma}_\Xi - \frac{3}{2}\,\bar{\sigma}^*_\Xi + \bar{\sigma}_\Xi\,\bar{\sigma}^*_\Xi}{C_\Xi}, \tag{38}$$

where

$$C_\Xi = 2 + \frac{1}{2}\,(1 - \bar{\sigma}_\Xi)\,\bar{\sigma}^*_\Xi. \tag{39}$$

Because $\bar{\sigma}^*_\Xi$ is also expressed by $\bar{\sigma}^*_\Lambda$, Eqs. (36)-(39) are also the functions of m^*_N and m^*_Λ.

Consequently, the scalar mean-fields, the effective masses and the renormalized coupling constants of baryons in Eq. (18) depend only on m^*_N and m^*_Λ. Therefore the properties of SHM are determined by these two values, which are the solutions of the self-consistency equations obtained by extremizing Eq. (18):

$$\begin{aligned}
\frac{\partial}{\partial\, M^*_N}\left(\frac{\mathcal{E}}{\rho_T}\right) \;=\; & \sum_B \frac{\partial\, M^*_B}{\partial\, M^*_N}\,\frac{\rho_{BS}}{\rho_T} + \frac{m^2_\sigma\,\langle\sigma\rangle}{M_N\,\rho_T}\,\frac{\partial\,\langle\sigma\rangle}{\partial\, m^*_N} + \frac{m^2_{\sigma^*}\,\langle\sigma^*\rangle}{M_N\,\rho_T}\,\frac{\partial\,\langle\sigma^*\rangle}{\partial\, m^*_N} \\
& + \frac{\rho_T}{M_N\, m^2_\omega}\left(\sum_B f_B\, g^*_{BB\omega}\right)\left(\sum_B f_B\,\frac{\partial\, g^*_{BB\omega}}{\partial\, m^*_N}\right) \\
& + \frac{\rho_T}{M_N\, m^2_\phi}\left(\sum_Y f_Y\, g^*_{YY\phi}\right)\left(\sum_Y f_Y\,\frac{\partial\, g^*_{YY\phi}}{\partial\, m^*_N}\right) = 0,
\end{aligned} \tag{40}$$

$$\begin{aligned}
\frac{\partial}{\partial\, M^*_\Lambda}\left(\frac{\mathcal{E}}{\rho_T}\right) \;=\; & \sum_B \frac{\partial\, M^*_B}{\partial\, M^*_\Lambda}\,\frac{\rho_{BS}}{\rho_T} + \frac{m^2_{\sigma^*}\,\langle\sigma^*\rangle}{M_\Lambda\,\rho_T}\,\frac{\partial\,\langle\sigma^*\rangle}{\partial\, m^*_\Lambda} \\
& + \frac{\rho_T}{M_\Lambda\, m^2_\omega}\left(\sum_B f_B\, g^*_{BB\omega}\right)\left(\sum_Y f_Y\,\frac{\partial\, g^*_{YY\omega}}{\partial\, m^*_\Lambda}\right) \\
& + \frac{\rho_T}{M_\Lambda\, m^2_\phi}\left(\sum_Y f_Y\, g^*_{YY\phi}\right)\left(\sum_Y f_Y\,\frac{\partial\, g^*_{YY\phi}}{\partial\, m^*_\Lambda}\right) = 0,
\end{aligned} \tag{41}$$

where $\rho_T = \sum \rho_B$ is the total baryon density and $f_B = \rho_B/\rho_T$ is the fraction of each

baryon and ρ_{BS} is the scalar density. The solutions of Eqs. (40) and (41) must satisfy the energy minimization conditions $\partial^2\mathcal{E}/\partial m_N^{*2} > 0$ and $(\partial^2\mathcal{E}/\partial m_N^{*2})(\partial^2\mathcal{E}/\partial m_\Lambda^{*2}) - (\partial^2\mathcal{E}/\partial m_N^* \partial m_\Lambda^*)^2 > 0$. Because it is tedious but straightforward task to calculate the derivatives in Eqs. (40) and (41), we will not present their expressions explicitly.

3 Numerical analyses

Here we calculate the properties of charge symmetric SHM consisting of baryon octet. The system is in chemical equilibrium under the conservations of the total baryon density (number) and the strangeness fraction (number) [18]. The chemical potentials μ_B of each baryon with strangeness S_B can be related to the baryon and the strangeness chemical potentials, μ_N and μ_S as

$$\mu_B = \mu_N + S_B\,\mu_S. \tag{42}$$

In the RMF model the μ_B is given by

$$\mu_B = \left[k_{FB}^2 + (M_B^*)^2\right]^{1/2} + V_B, \tag{43}$$

where k_{FB} is the Fermi momentum of each baryon and V_B is given by Eq. (15). Because the r.h.s. of Eq. (43) contains the effective mass of each baryon, a set of equations (40)-(43) have to be solved self-consistently.

Before performing actual calculations, we have to specify the free (un-renormalized) meson-baryon coupling constants. The $NN\sigma$ and $NN\omega$ coupling constants were determined to reproduce the nuclear matter saturation properties in Ref. [13]. The nucleon-hyperon (NY) and hyperon-hyperon (YY) interactions however are not well known at present. We first determine them according to Ref. [18]. The $YY\omega$ coupling constants are fixed by the SU(6) relations:

$$\frac{1}{3}\,g_{NN\omega} = \frac{1}{2}\,g_{\Lambda\Lambda\omega} = \frac{1}{2}\,g_{\Sigma\Sigma\omega} = g_{\Xi\Xi\omega}. \tag{44}$$

On the other hand, the $YY\sigma$ coupling constants are chosen to reproduce reasonable hyperon potentials in saturated nuclear matter:

$$U_\Lambda^{(N)}(\rho_{nm}) = -28\,\mathrm{MeV}, \quad U_\Sigma^{(N)}(\rho_{nm}) = 30\,\mathrm{MeV} \quad \text{and} \quad U_\Xi^{(N)}(\rho_{nm}) = -18\,\mathrm{MeV}, \tag{45}$$

where the potential $U_Y^{(N)}$ is given by a simple summation of the scalar S_Y and vector V_Y potentials and $\rho_{nm} = 0.16\,\mathrm{fm}^{-3}$ is the saturation density. The obtained values are

$$\frac{g_{\Lambda\Lambda\sigma}}{g_{NN\sigma}} = 0.604, \quad \frac{g_{\Sigma\Sigma\sigma}}{g_{NN\sigma}} = 0.461 \quad \text{and} \quad \frac{g_{\Xi\Xi\sigma}}{g_{NN\sigma}} = 0.309. \tag{46}$$

The $YY\phi$ coupling constants are also fixed by the SU(6) relations:

$$2\,g_{\Lambda\Lambda\phi} = 2\,g_{\Sigma\Sigma\phi} = g_{\Xi\Xi\phi} = -\frac{2\sqrt{2}}{3}\,g_{NN\omega}. \tag{47}$$

Of course $g_{NN\phi} = 0$. The remaining $YY\sigma^*$ coupling constants are adjusted so that the potential of a single hyperon, embedded in a bath of Ξ matter at ρ_{nm}, becomes

$$U_\Xi^{(\Xi)}(\rho_{nm}) = U_\Lambda^{(\Xi)}(\rho_{nm}) = -40\,\mathrm{MeV}. \tag{48}$$

The obtained values are

$$\frac{g_{\Lambda\Lambda\sigma^*}}{g_{NN\sigma}} = \frac{g_{\Sigma\Sigma\sigma^*}}{g_{NN\sigma}} = 0.690 \quad \text{and} \quad \frac{g_{\Xi\Xi\sigma^*}}{g_{NN\sigma}} = 1.22, \tag{49}$$

where $g_{\Sigma\Sigma\sigma^*} = g_{\Lambda\Lambda\sigma^*}$ is assumed according to SU(6) symmetry. These values predict the following potential of a single hyperon embedded in a Λ bath at ρ_{nm}:

$$U_\Lambda^{(\Lambda)}(\rho_{nm}) \approx U_\Xi^{(\Lambda)}(\rho_{nm}) \approx -20\,\mathrm{MeV}. \tag{50}$$

It is seen that the $\Lambda\Lambda$ interaction is rather attractive. Hereafter we call the model developed in the present work with strange mesons as extended ZM (EZM) model so as to distinguish it from the MZM model in Ref. [13] without strange mesons. The EZM model using the coupling constants determined above is especially called as EZM1.

Then we present the properties of SHM calculated by EZM1. Figure 1 shows the binding energies per baryon

$$\frac{E}{A} = \frac{\varepsilon}{\rho_T} - \sum_{B=N,\Lambda,\Sigma,\Xi} f_B\,M_B, \tag{51}$$

as functions of the total baryon density ρ_T for several fixed strangeness fractions:

$$f_S = f_\Lambda + f_\Sigma + 2f_\Xi. \tag{52}$$

The results suggest that the SHM with $f_S \approx 1$ becomes the most stable form of baryon matter at $\rho_T \approx 0.4\,\mathrm{fm}^{-3}$. In order to examine it in detail, Fig. 2 calculates the lowest binding energies per baryon as functions of the strangeness fraction. The result of EZM1 is shown by the solid curve. We have found that the SHM with $f_S = 1.14$ is the most stable state of $E/A = -18.2\,\mathrm{MeV}$ The NLW model [18] predicts the maximum binding energy 24.6 MeV at $f_S = 1.3$ while the QMC model [19] predicts lower energy 19 MeV at less strangeness fraction $f_S = 1.2$. Our result generally agrees with the QMC model rather than the NLW model, but predicts the even lower binding energy at even lower strangeness fraction than the QMC. This indicates the importance of the medium dependences of meson-baryon coupling constants.

The dip of $E/A = -16.2\,\mathrm{MeV}$ at $f_S = 0.095$ is the most stable state of the SHM consisting of N and Λ only. So as to make this clear, the result of $N + \Lambda$ matter is shown by the dashed curve. The $N + \Lambda$ system becomes less stable than $N + \Lambda + \Sigma + \Xi$ system as the strangeness fraction increases and eventually becomes unbound at $f_S = 0.72$. The dotted curve shows the result by MZM taking into account all the baryon octets. In this case the most stable state is $N + \Lambda$ matter that has the energy $E/A = -16.1\,\mathrm{MeV}$ at $f_S = 0.077$. The absence of attractive interaction between s quarks predicts less stable state than EZM1 at higher strangeness fraction and then leads to unbound state above $f_S = 1.450$.

The black curves in Fig. 3 show the corresponding particle fractions f_B to the lowest energy of the solid curve in Fig. 2 as functions of the strangeness fraction. The Σ's are absent owing to the repulsive potential adopted in Eq. (45). In the following there are no contributions of Σ in the results of EZM1. The nucleons decrease monotonically as f_S increases and disappear above $f_S = 1.75$. The Ξ's appear at $f_S = 0.20$ and increase monotonically as f_S increases. At $f_S = 1.0$ the fractions of N and Ξ have the same values $f_N = f_\Xi = 0.38$. The Λ's always appear except for $f_S = 0.0$ and $f_S = 2.0$. Owing to the strangeness conservation, the fraction of Λ increases rapidly before the appearance of Ξ's and then gradually up to its maximum value $f_\Lambda = 0.249$ at $f_S = 1.725$. As soon as the nucleons disappear, the Ξ's increase rapidly because of the baryon number conservation and so the Λ's turn to decrease because of the strangeness conservation. Consequently, the disappearance of nucleons gives rise to the kink on the solid curve at $f_S = 1.75$ in Fig. 2.

The solid and dashed-dotted curves in Fig. 4 show the total baryon densities corresponding to the energies by EZM1 and MZM in Fig. 2. The strange mesons have effect to increase the density for each value of the strangeness fraction. As the strangeness grows, both the densities increase up to their maximum values $\rho_T = 0.43\,\mathrm{fm}^{-3}$ at $f_S = 1.41$ and $\rho_T = 0.33\,\mathrm{fm}^{-3}$ at $f_S = 1.30$ and then turn to decrease. The kink on the solid curve at $f_S = 1.75$ reflects the disappearance of nucleons again. It is seen that the most stable state of $N+\Lambda+\Xi$ system with $f_S = 1.14$ appears at $\rho_T = 0.39\,\mathrm{fm}^{-3}$. Without the strange mesons we cannot find the chemical-equilibrated state above $f_S = 1.55$.

The black curves in Fig. 5 calculate the potential $U_B = S_B + V_B$ of each baryon corresponding to the solid curve in Fig. 2. The solid, dashed and dotted curves are the results for N, Λ and Ξ respectively. The U_Λ and U_Ξ are almost the same because they are determined to satisfy Eq. (48). Below $f_S = 1.4$ the U_N is much deeper than U_Λ and U_Ξ while above $f_S = 1.6$ it becomes shallower. The U_N becomes deepest around $f_S = 1.0$ while the U_Λ and U_Ξ become deepest around $f_S = 1.5$. Consequently, the value of f_S, at which the most stable SHM appears, shifts to the somewhat larger value than 1 as seen above.

The properties of SHM have been determined by solving self-consistency equations (40) and (41) for the effective masses of N and Λ under the chemical equilibrium (42)

constrained by the strangeness conservation. As a result, the effective mass of each baryon $m_B^* = M_B^*/M_B$ implicitly depends on the strangeness. The black curves in Fig. 6 show the effective masses corresponding to the solid curve in Fig. 2. The solid, dashed and dotted curves are the results for N, Λ and Ξ respectively. Below $f_S = 1.5$ the masses of the baryons with lower strangeness are reduced more significantly because of the dominance of $\langle\sigma\rangle$ mean-field over $\langle\sigma^*\rangle$. On the other hand, above $f_S = 1.7$ the masses of the baryons with higher strangeness are reduced more significantly because of the dominance of $\langle\sigma^*\rangle$ over $\langle\sigma\rangle$. It is noted that the minimum of m_N^* appears at $f_S = 1.16$ being almost the same as $f_S = 1.14$. This indicates that the most stable SHM is still dominated by $\langle\sigma\rangle$ mean-field.

The renormalized coupling constants also reflect the strangeness. The black curves in Figs. 7 and 8 calculate $g^*_{BB\sigma(\omega)}/g_{BB\sigma(\omega)}$ and $g^*_{YY\sigma^*(\phi)}/g_{YY\sigma(\omega)}$ corresponding to the solid curve in Fig. 2. Their essential behaviors are determined by the numerators in Eqs. (28), (29), (36) and (37). Therefore the strangeness fractions on the minimums of $g^*_{\Lambda\Lambda\sigma(\omega)}$ and $g^*_{\Lambda\Lambda\sigma^*(\phi)}$ are almost the same as those of M^*_Ξ and M^*_N respectively.

So far we have used the $YY\sigma^*$ coupling constants determined through Eq. (48). However the recent discovery of ${}^{\ 6}_{\Lambda\Lambda}$He in the KEK-E373 experiment [20] has presented a question on the strong $\Lambda\Lambda$ attraction in Eq. (50). In this respect we cannot regard the values of Eq. (49) to be physically proper. At present there remain some ambiguities in determining the $YY\sigma^*$ coupling constants. Therefore Refs. [18] and [19] investigated the properties of SHM using the most recent SU(3)-extension NSC97f [21,22] of the Nijmegen soft-core potential model as well. In fact the new result of ${}^{\ 6}_{\Lambda\Lambda}$He was reproduced by the calculation [23] based on the three-body Faddeev equation and the NSC97 potential. Unfortunately it cannot be directly used in the RMF models and so was implemented [18] by adjusting the $YY\sigma^*$ coupling constants to reproduce the hyperon binding energy curves in Fig. 2 of Ref. [24]. This method of implementation still has problems. First the quantitatively satisfactory agreements with the energies were not obtained [18,19] by any adjustment of the $YY\sigma^*$ coupling constants in the RMF models. More seriously, Ref. [24] employed the NRBHF model that is essentially different from the RMF models and so was not able to reproduce the nuclear matter saturation properties. Therefore we cannot say that the above implementation precisely takes into account the YY interactions of NSC97f potential.

In spite of these problems, for completeness of the comparison between our EZM model and the NLW and QMC models, we also calculate the properties of SHM using the YY interactions of NSC97f potential implemented by the same way as Ref. [18] into EZM model. Figure 9 shows the binding energy per baryon in its own baryonic matter. We have used the following $YY\sigma^*$ coupling constants in place of Eq. (49):

$$\frac{g_{\Lambda\Lambda\sigma^*}}{g_{NN\sigma}} = 0.52, \quad \frac{g_{\Sigma\Sigma\sigma^*}}{g_{NN\sigma}} = 0.96 \quad \text{and} \quad \frac{g_{\Xi\Xi\sigma^*}}{g_{NN\sigma}} = 1.28. \tag{53}$$

$U_\Sigma^{(N)}(\rho_{nm})$ in Eq. (45) has been reduced to 20 MeV and we have $g_{\Sigma\Sigma\sigma}/g_{NN\sigma} = 0.485$ so that the binding energy of pure Σ matter agrees with the result of Ref. [24] more precisely than those in Refs. [18] and [19]. However the agreement with the pure Ξ matter cannot be improved by any reasonable adjustments of the relevant quantities. This suggests again the essential difference between NRBHF and RMF models. We call the EZM model using the $YY\sigma^*$ coupling constants of Eq. (53) as EZM2.

Then Fig. 10 calculates the lowest binding energies per baryon as functions of the strangeness fraction again. The solid curve is the result of EZM2. For the comparison the result of EZM1 is also shown by the dotted curve. The difference between the two models is small below $f_S = 1.0$ while the energy by EZM2 becomes much larger above $f_S = 1.0$. The deep bound state by the YY interactions of NSC97f potential has been attributed [18] to the first-order phase transition from the SHM consisting of $N + \Lambda + \Xi$ to the SHM with Σ-dominance. This has been also confirmed in our model. The black curves in Fig. 11 show the corresponding particle fractions to the solid curve in Fig. 10. As soon as the strangeness fraction crosses over 1.0, the Σ's suddenly appear and increase and so the other baryons rapidly decrease because of the baryon number and strangeness conservations. The N and Λ disappear above $f_S = 1.2$. Although the results of EZM2 generally agree with Refs. [18] and [19], there are a few differences that our binding energy of the most stable state is deeper than the QMC model and that the Σ-dominance in our calculation is more conspicuous than the NLW model. The dotted curve in Fig. 4 shows the total baryon density corresponding to the solid curve in Fig. 10. We can see clearly the discontinuity of the density at $f_S = 1.06$ due to the first-order phase transition.

The $\Sigma\Sigma$ interaction in NSC97f is strongly attractive. However it has been never confirmed experimentally at present. Therefore we consider another model EZM3 in which $\Sigma\Sigma\sigma^*$ coupling constant is assumed to be the same as $\Lambda\Lambda\sigma^*$, $g_{\Sigma\Sigma\sigma^*}/g_{NN\sigma} = 0.52$, according to SU(6) symmetry and the $\Sigma\Sigma\sigma$ coupling constant is the same as Eq. (46). The other coupling constants are the same as EZM2. The lowest binding energy per baryon is shown by the dashed curve in Fig. 10 and the corresponding particle fractions are shown by the blue curves in Fig. 11. For the comparison with EZM1, the particle fractions are also shown by the blue curves in Fig. 3. There appear no Σ's in the results of EZM3, which are the same as EZM2 before the appearance of Σ's in it at $f_S = 1.06$. The EZM3 predicts the most stable state of SHM of $E/A = -24.8\,\mathrm{MeV}$ at $f_S = 1.57$. The strangeness fraction is larger than EZM1 and EZM2 because the SHM by EZM3 is dominated by Ξ hyperons. The fraction of Ξ's in Fig. 3 or 11 increases linearly as the strangeness fraction becomes larger. The nucleons do not disappear below $f_S = 2.0$. The Λ gradually decreases above $f_S = 0.2$ and disappears at $f_S = 1.875$ because of much weaker $\Lambda\Lambda$ attraction than EZM1.

The differences in the strength of $\Lambda\Lambda$ attraction and Ξ abundance between EZM1 and EZM3 are clearly seen in the dashed and dotted curves of Fig. 5. The U_Λ and U_Ξ

by EZM3 are much shallower and deeper respectively than those by EZM1 at higher strangeness fraction. For the most stable SHM by EZM3, the U_Ξ becomes deeper than U_N. The dashed curve in Fig. 4 shows the total baryon density corresponding to the dashed curve in Fig. 10. Below $f_S = 1.06$ it is connected to the dotted curve. The maximum density $\rho_T = 0.45\,\mathrm{fm}^{-3}$ appears at $f_S = 1.51$ being close to $f_S = 1.57$. The effective masses and renormalized coupling constants corresponding to the dashed curve in Fig. 10 are shown by the blue curves in Figs. 6, 7 and 8. Their minimums shift to larger strangeness fractions than the black curves by EZM1. These results are also because the most stable SHM by EZM3 is dominated by Ξ abundance.

4 Summary

Introducing the (hidden) strange mesons into the modified Zimanyi-Moszkowski model developed previously in Ref. [13], we have extended it further so as to investigate dense strange baryonic matter accurately. The model is based on the constituent quark picture of baryons. Taking into account the effect of scalar potential on the constituent quarks, the medium corrections to meson-baryon couplings are derived. The resultant renormalized coupling constants effectively depend on the density through the effective masses of baryons in medium.

Because at present there is little reliable information on the hyperon-hyperon interactions, the three possibilities have been investigated. The first one (EZM1) is designed so that the $YY\sigma^*$ coupling constants are adjusted to reproduce the empirical potential of a single hyperon embedded in a bath of Ξ matter at nuclear saturation density. We have found the most stable form of baryonic matter, whose binding energy $E/A = -18.2\,\mathrm{MeV}$ and strangeness fraction $f_S = 1.14$ are similar to those obtained by the QMC model but are lower than the NLW model. This indicates the importance of medium-dependent meson-baryon coupling constants in dense baryon matter.

The second model (EZM2) is designed to implement the Nijmegen soft-core potential model NSC97f. As well as the NLW and QMC models, we have found the phase transition from the SHM consisting of $N + \Lambda + \Xi$ to that with Σ-dominance, when the strangeness fraction becomes larger than $f_S = 1.0$. This is due to the strongly attractive $\Sigma\Sigma$ interaction in NSC97f potential. The obtained binding energy of the most stable SHM is deeper than the QMC model. This indicates the differences between EZM and QMC models in the medium dependences of meson-baryon effective coupling constants.

Because the strong $\Sigma\Sigma$ interaction in NSC97f potential has not been confirmed, the third model (EZM3) reduces the $\Sigma\Sigma\sigma^*$ coupling constant in EZM2 to the same value as $\Lambda\Lambda\sigma^*$ coupling. The resulting SHM is dominated by abundance of Ξ hyperons and so the most stable state has larger strangeness fraction than EZM1 and EZM2.

In conclusion our new extended ZM model works well to describe the dense SHM as well as the most refined NLW and the modified QMC models. However we have

found important non-negligible differences between them. This indicates that the precise consideration of the medium dependences of effective meson-baryon coupling constants is important to describe dense baryon matter as neutron star matter correctly. Although at present there is no reliable empirical information on the medium dependence at high densities, the EZM model with reasonable baryon-baryon interactions provides a useful instrument to investigate dense baryon matter.

References

[1] B.D. Serot and J.D. Walecka, *Advances in Nuclear Physics*, Vol. **16** (Plenum, New York, 1986).

[2] S. Gmuca, Nucl. Phys. **A547** (1992) 447.

[3] F. Hofmann, C.M. Keil and H. Lenske, Phys. Rev. **C64** (2001) 025804, [arXiv:nucl-th/0008038].

[4] R. Brockmann and R. Machleidt, Phys. Rev. **C42** (1990) 1965.

[5] M. Baldo, G.F. Burgio and H.-J. Schulze, Phys. Rev. **C61** (2000) 055801, [arXiv:nucl-th/9912066].

[6] I. Vidaña, A. Polls, A. Ramos, L. Engvik and M. Hjorth-Jensen, Phys. Rev. **C62** (2000) 035801, [arXiv:nucl-th/0004031].

[7] P.A.M. Guichon, Phys. Lett. **B200** (1988) 235; K. Saito and A.W. Thomas, Phys. Lett. **B327** (1994) 9; Phys. Rev. **C52** (1995) 2789.

[8] J. Zimanyi and S.A. Moszkowski, Phys. Rev. **C42** (1990) 1416. It is noted that the NLW model has linear meson-baryon couplings in spite of its name. On the contrary, the DSC and QMC models are true nonlinear mean-field models.

[9] M. Barranco, R.J. Lombard, S. Marcos and S.A. Moszkowski, Phys. Rev. **C44** (1991) 178.

[10] N.K. Glendenning, F. Weber and S.A. Moszkowski, Phys. Rev. **C45** (1992) 844.

[11] K. Miyazaki, Prog. Theor. Phys. **91** (1994) 1271.

[12] K. Miyazaki, CERN Document Server (CDS) ext-2002-056 revised by Mathematical Physics Preprint Archive (mp_arc) 05-141.

[13] K. Miyazaki, CERN Document Server (CDS) ext-2003-062 revised by Mathematical Physics Preprint Archive (mp_arc) 05-178.

[14] K. Miyazaki, CERN Document Server (CDS) ext-2003-077 revised by Mathematical Physics Preprint Archive (mp_arc) 05-190.

[15] K. Miyazaki, CERN Document Server (CDS) ext-2004-010 revised by Mathematical Physics Preprint Archive (mp_arc) 05-199.

[16] K. Miyazaki, CERN Document Server (CDS) ext-2004-036 revised by Mathematical Physics Preprint Archive (mp_arc) 05-206.

[17] J. Schaffner, C.B. Dover, A. Gal, C. Greiner and H. Stöker, Phys. Rev. Lett. **71** (1993) 1328.

[18] J. Schaffner-Bielich and A. Gal, Phys. Rev. **C62** (2000) 034311, [arXiv:nucl-th/0005060].

[19] I. Zakout, H.R. Jaqaman, H. Stöker and W. Greiner, J. Phys. G27 (2001) 1939, [arXiv:nucl-th/005005].

[20] H. Takahashi *et al.*, Phys. Rev. Lett. **87** (2001) 212502.

[21] V.G.J. Stoks and Th.A. Rijken, Phys. Rev. **C59** (1999) 3009, [arXiv:nucl-th/9901028].

[22] Th.A. Rijken, V.G.J. Stoks and Y. Yamamoto, Phys. Rev. **C59** (1999) 21, [arXiv:nucl-th/9807082].

[23] I.N. Filikhin and A. Gal, Phys. Rev. **C65** (2002) 041001(R); Nucl. Phys. **A707** (2002) 491, [arXiv:nucl-th/0203036]; I.N. Filikhin, A. Gal and V.M. Suslov, Phys. Rev. **C68** (2003) 024002, [arXiv:nucl-th/0303028]; Nucl. Phys. **A743** (2004) 194, [arXiv:nucl-th/0406049];

[24] V.G.J. Stoks and T.-S.H. Lee, Phys. Rev. **C60** (1999) 024006, [arXiv:nucl-th/9901030].

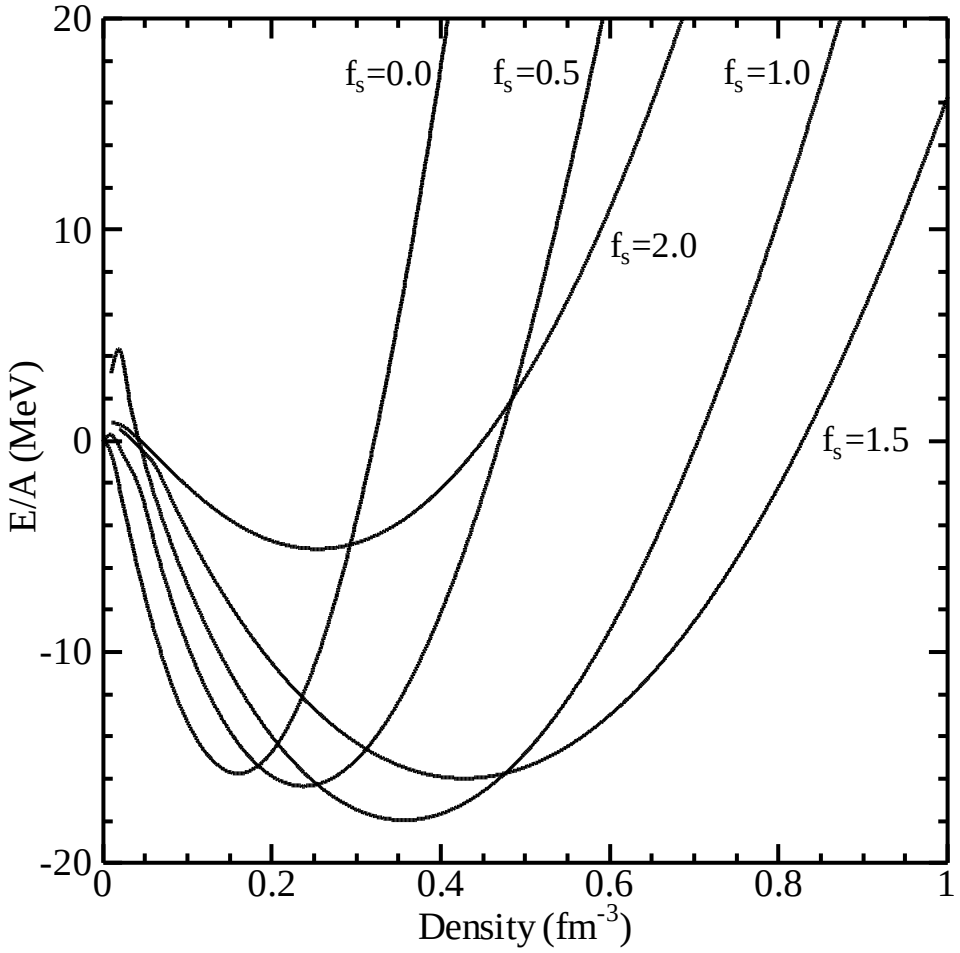

Figure 1: The binding energies per baryon by EZM1 as functions of the total baryon density for fixed strangeness fraction.

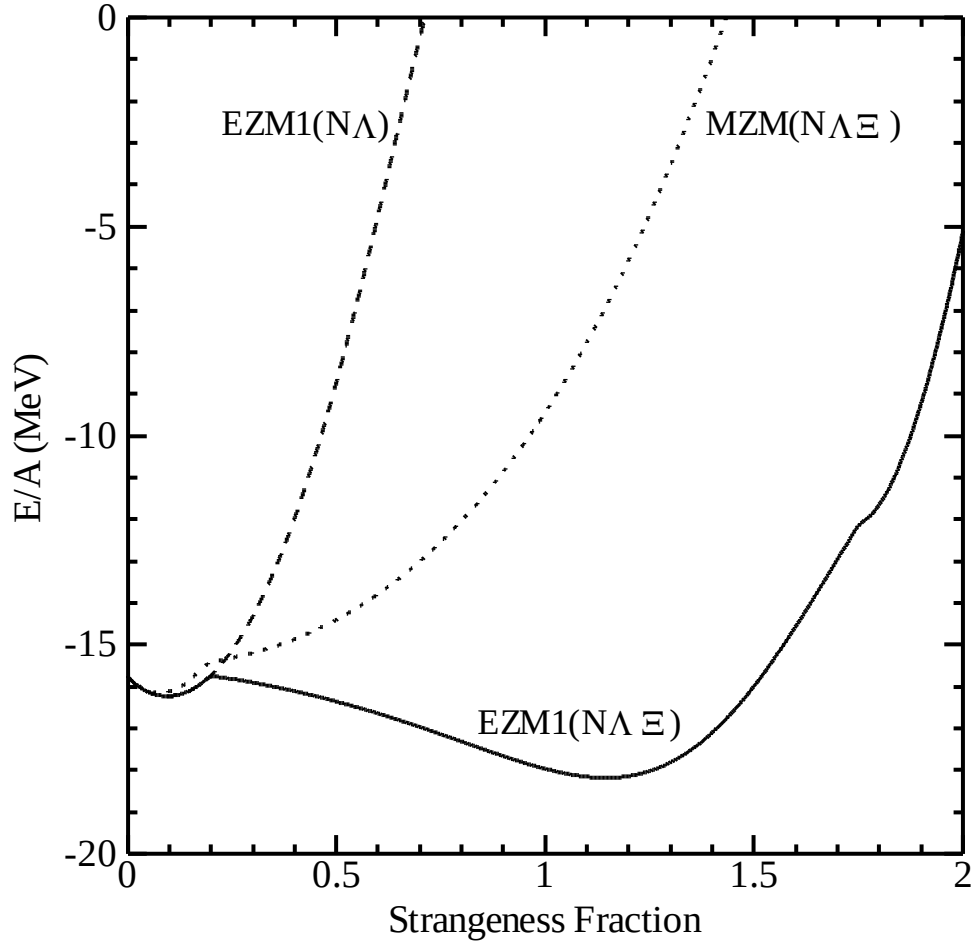

Figure 2: The lowest binding energies per baryon for each value of the strangeness fraction. The solid, dashed and dotted curves are the results using EZM1 including all the baryon octets, EZM1 including N and Λ only and MZM including all the baryons.

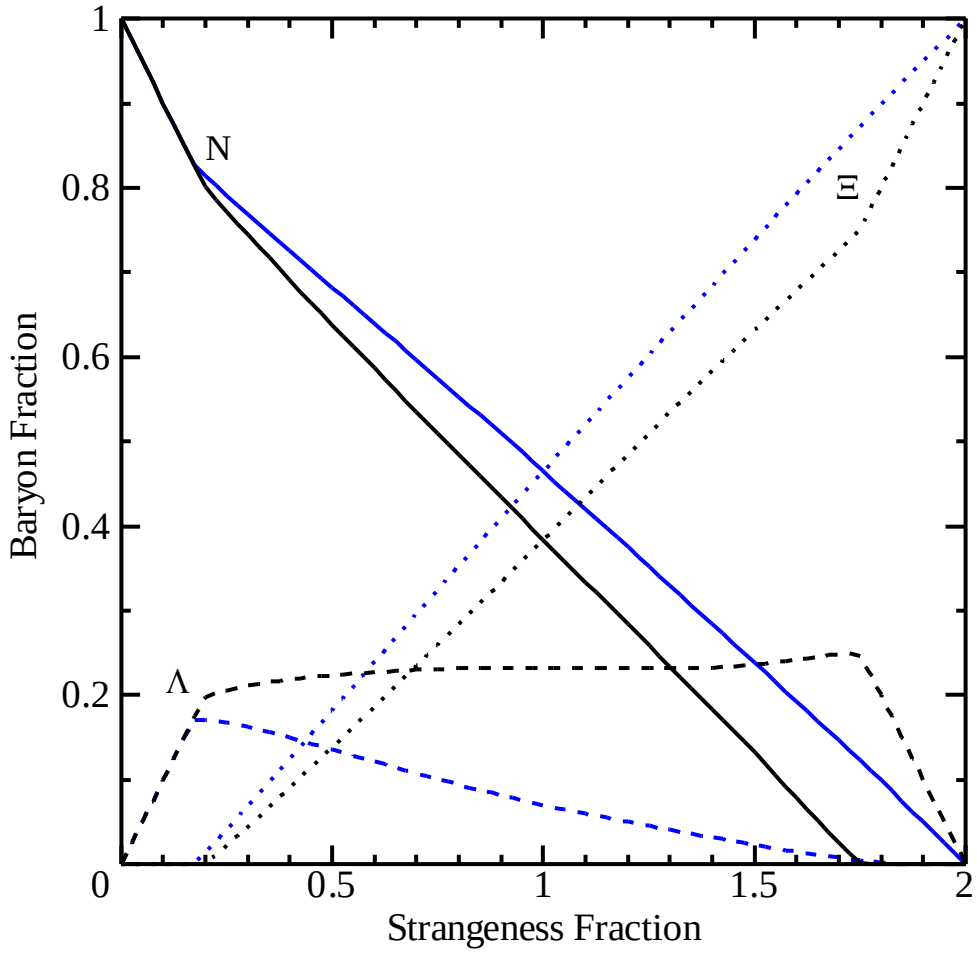

Figure 3: The black curves show the fractions of each baryon corresponding to the solid curve in Fig. 2. The blue curves show the results calculated by EZM3.

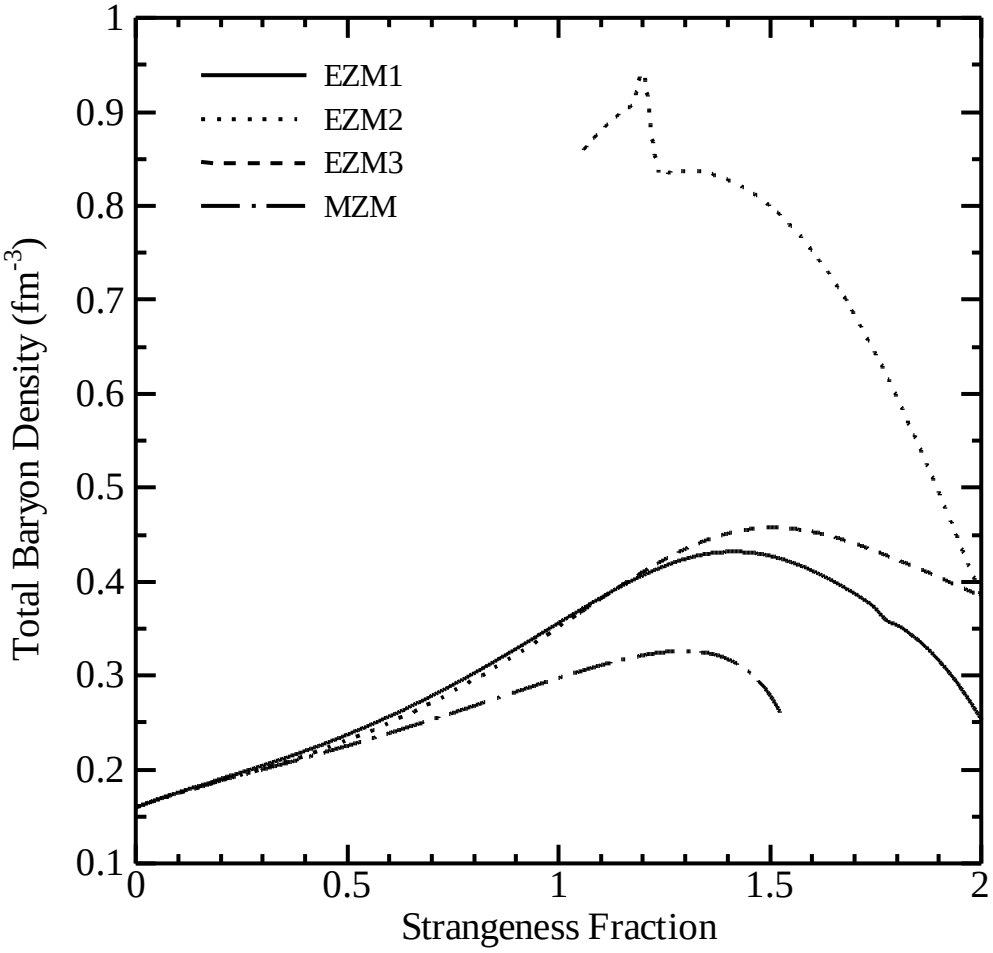

Figure 4: The solid and dashed-dotted curves show the total baryon densities corresponding to the solid and dotted curves in Fig. 2. The dotted and dashed curves show the results calculated by EZM2 and EZM3 respectively.

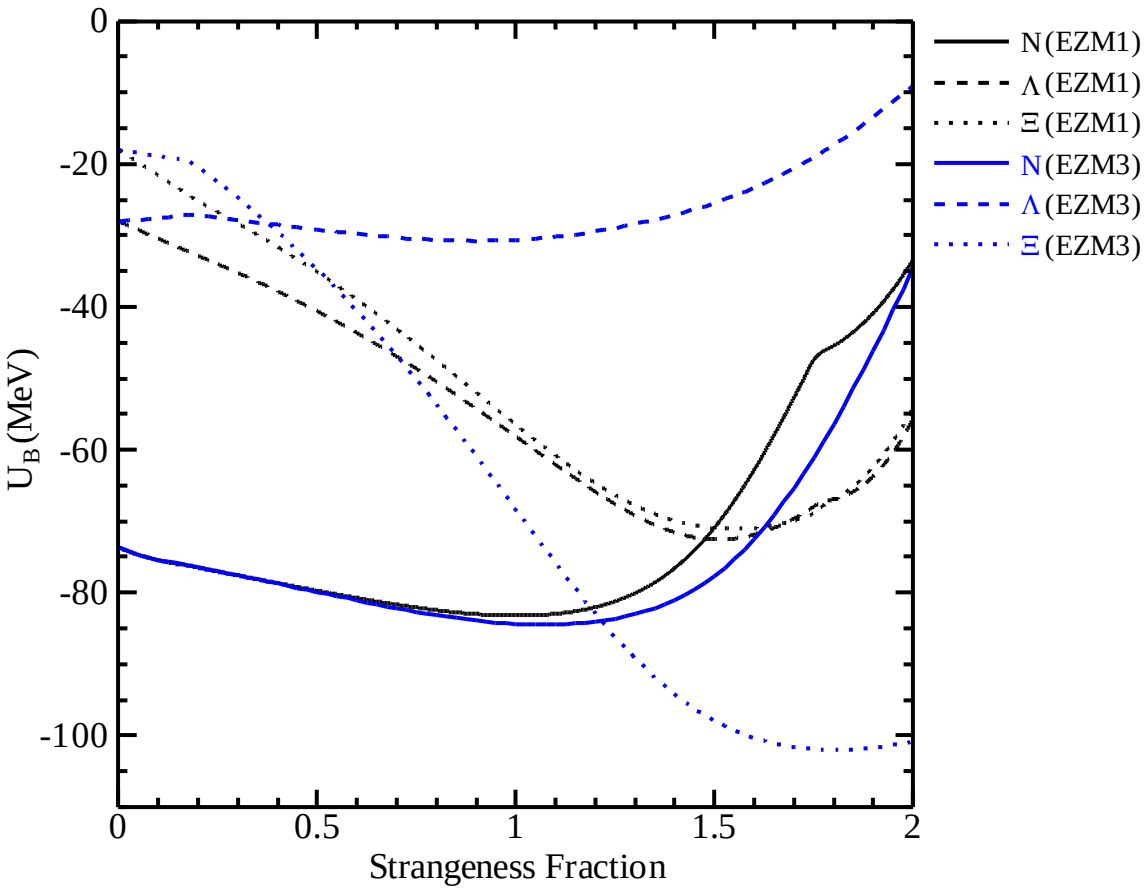

Figure 5: The black curves show the potential $U_B = S_B + V_B$ of each baryon corresponding to the solid curve in Fig. 2. The blue curves show the results calculated by EZM3.

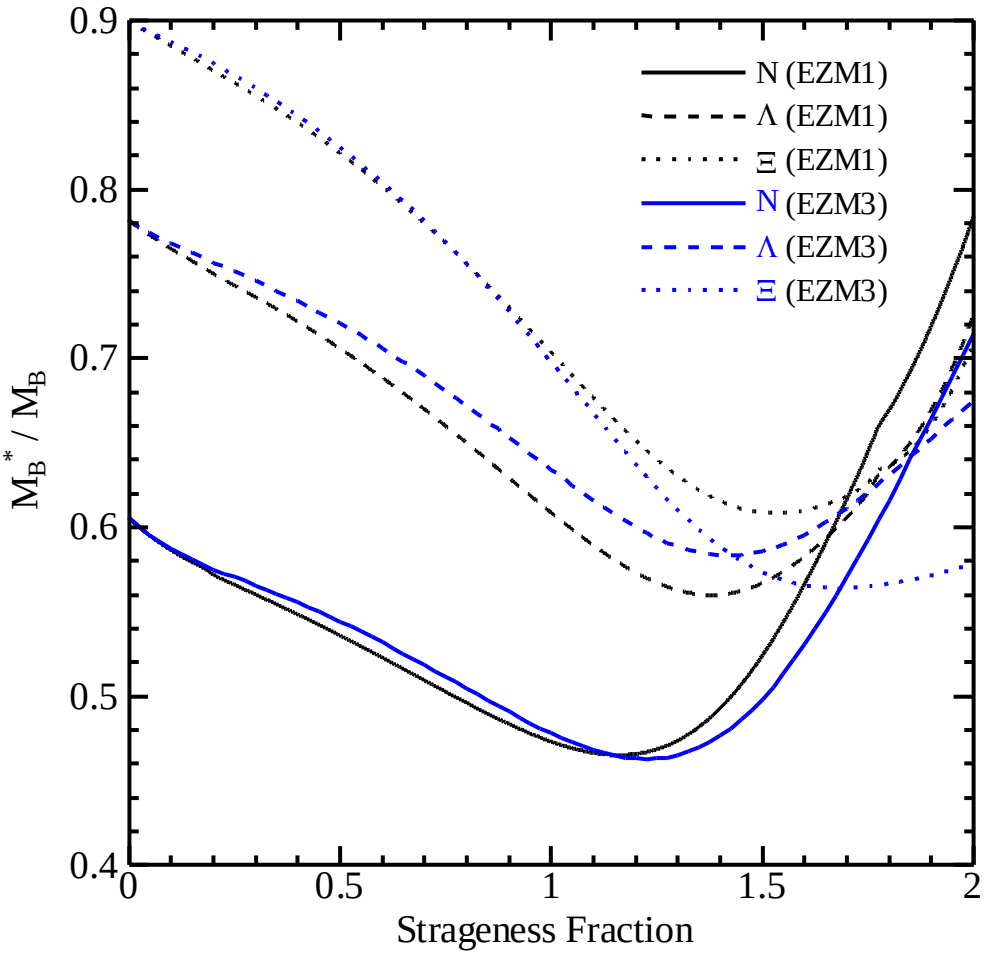

Figure 6: The black curves show the effective masses of each baryon corresponding to the solid curve in Fig. 2. The blue curves show the results calculated by EZM3.

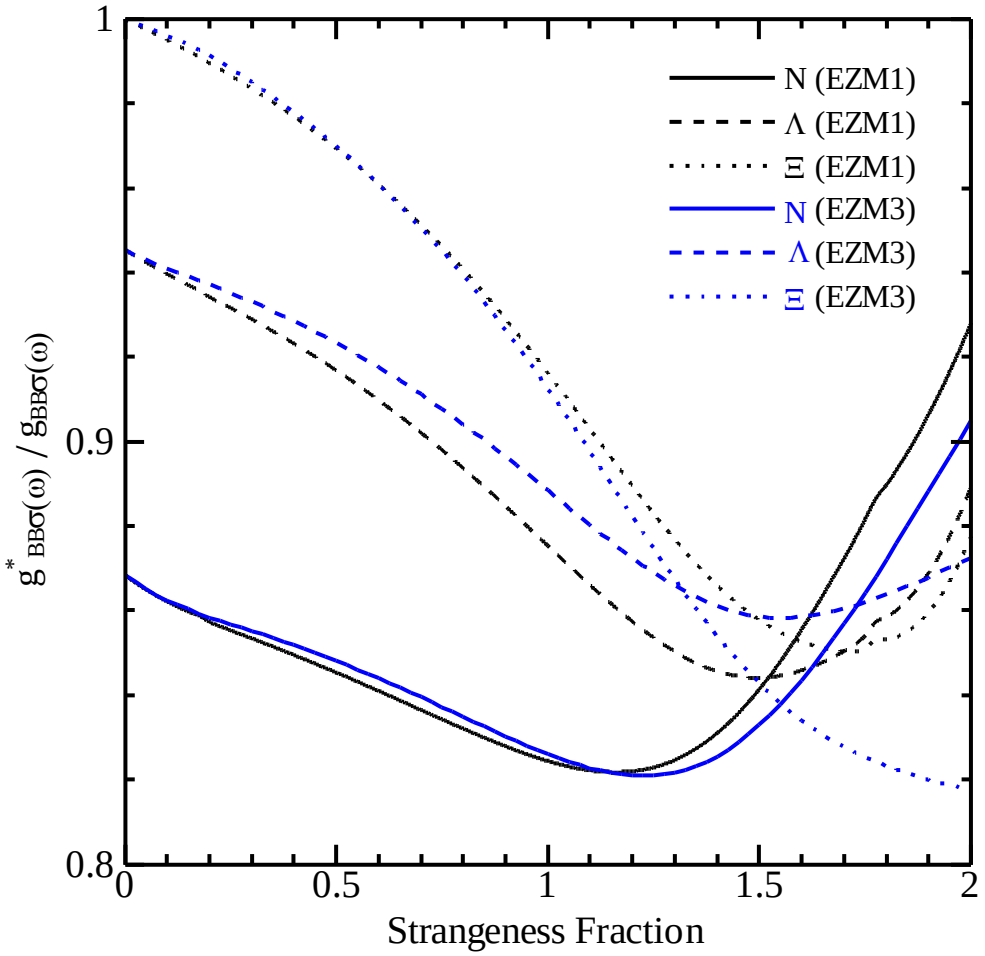

Figure 7: The black curves show the renormalized coupling constants $g^*_{BB\sigma(\omega)}/g_{BB\sigma(\omega)}$ corresponding to the solid curve in Fig. 2. The blue curves show the results calculated by EZM3.

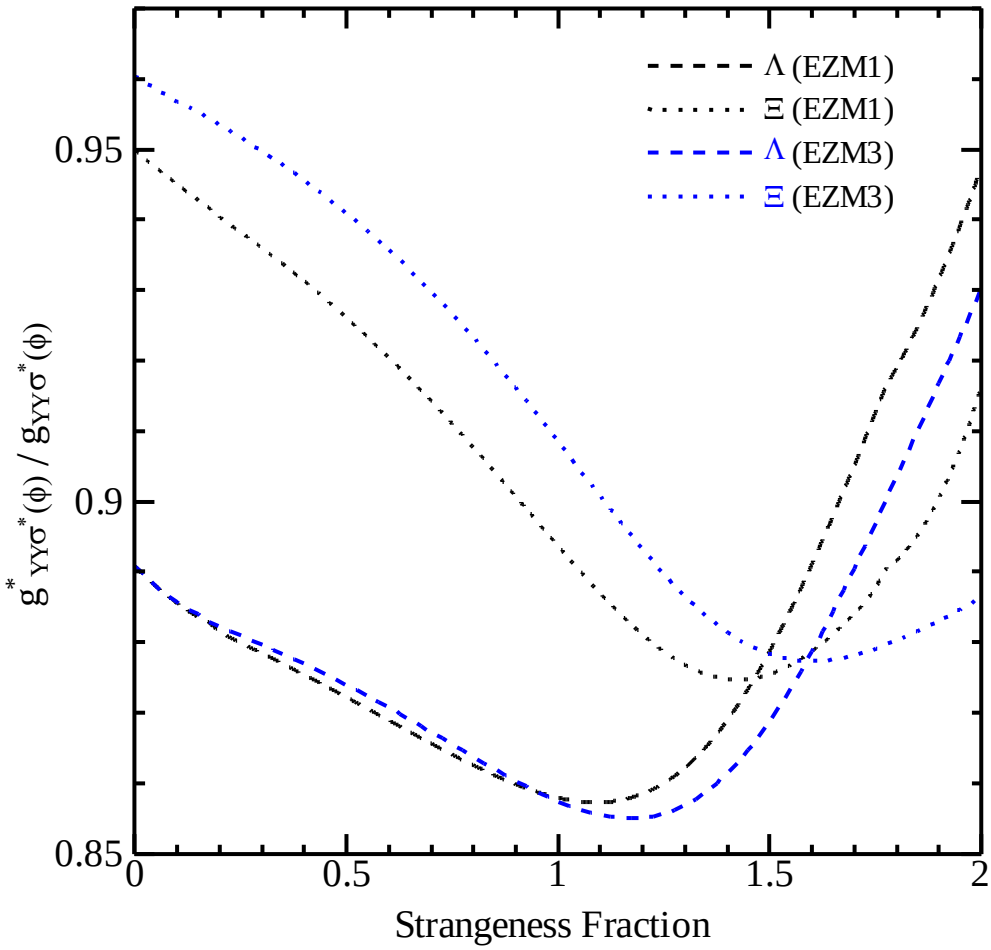

Figure 8: The black curves show the renormalized coupling constants $g^*_{YY\sigma^*(\phi)}/g_{YY\sigma^*(\phi)}$ corresponding to the solid curve in Fig. 2. The blue curves show the results calculated by EZM3.

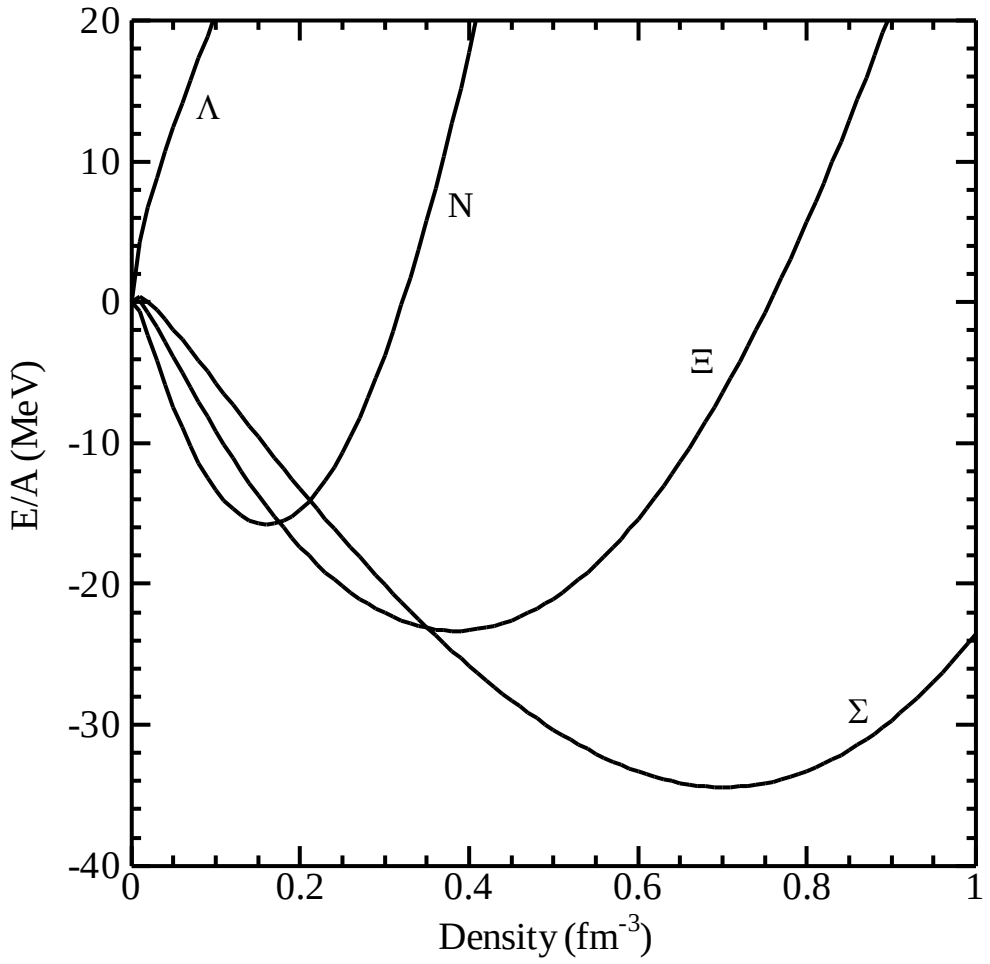

Figure 9: The binding energy per baryon in its own baryonic matter using $YY\sigma^*$ coupling constants of EZM2.

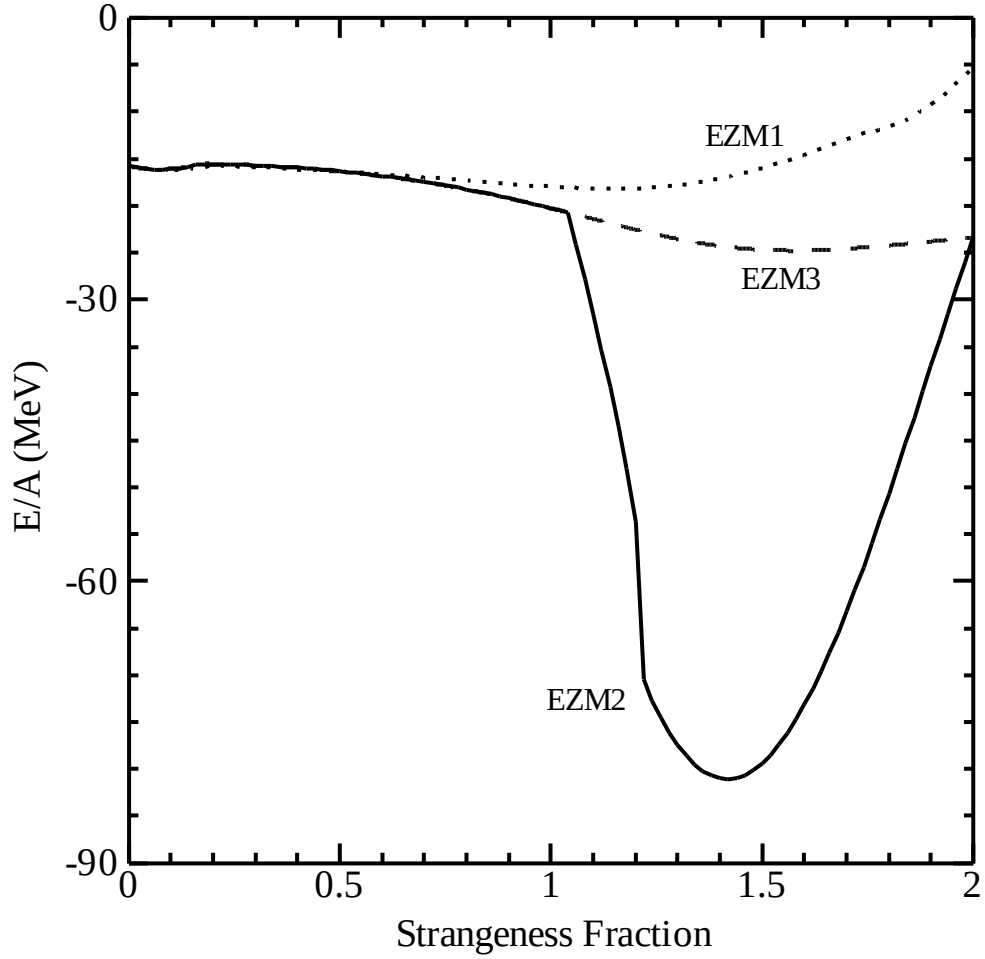

Figure 10: The lowest binding energies per baryon as functions of the strangeness fraction.

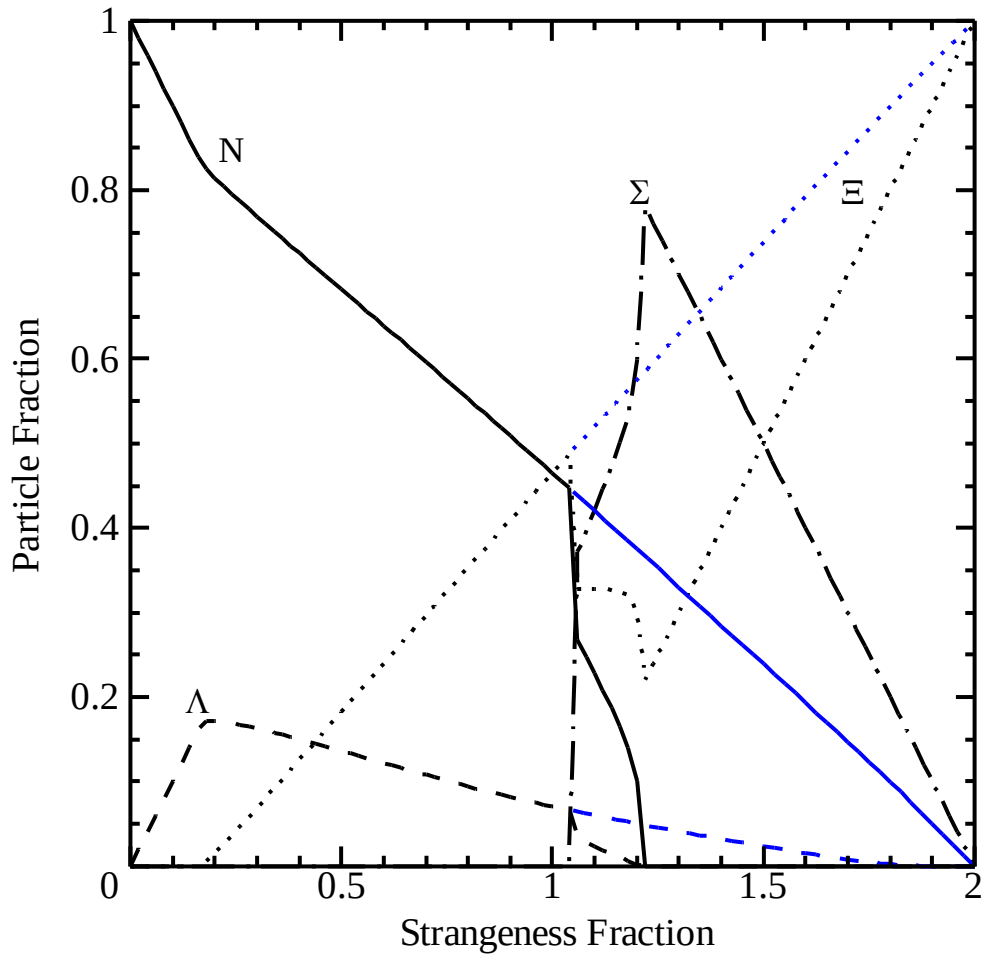

Figure 11: The fractions of each baryon corresponding to the lowest binding energy of EZM2 (black curves) and EZM3 (blue curves) in Fig. 10.